



# Kernel adaptive filtering-based phase noise compensation for pilot-free optical phase conjugated coherent systems

SONIA BOSCOLO,<sup>1,\*</sup>  TU T. NGUYEN,<sup>1,2</sup> ABDALLAH A. I. ALI,<sup>1</sup>   
STYLIANOS SYGLETOS,<sup>1</sup> AND ANDREW D. ELLIS<sup>1</sup> 

<sup>1</sup>*Aston Institute of Photonic Technologies, Aston University, Birmingham B4 7ET, United Kingdom*

<sup>2</sup>*Currently with Infinera PA, 7360 Windsor Dr, Allentown, PA 18106, USA*

\**s.a.boscolo@aston.ac.uk*

**Abstract:** We propose a kernel-based adaptive filtering method to suppress the phase noise (PN) arising from small deviations from ideal counter-phasing in the dual-pump fibre-based optical phase conjugation (OPC) of pilot-free quadrature-amplitude modulation (QAM) signals. We demonstrate experimentally and numerically that the proposed scheme achieves signal-to-noise ratio improvement over conventional PN compensation under optimised pump dithering settings in the OPC device and features no performance penalty across a range of pump-phase mismatch values, when it is used with a 16-QAM signal in an optical back-to-back configuration. We also illustrate the applicability of the method to the 64-QAM modulation format, and evaluate its performance in a transmission setup with mid-link OPC by means of numerical simulations.

Published by Optica Publishing Group under the terms of the [Creative Commons Attribution 4.0 License](https://creativecommons.org/licenses/by/4.0/). Further distribution of this work must maintain attribution to the author(s) and the published article's title, journal citation, and DOI.

## 1. Introduction

Optical phase conjugation (OPC) has shown to be a promising method for the simultaneous compensation of the accumulated chromatic dispersion and distortion due to fibre Kerr nonlinearities in coherent optical systems [1–3]. In fibre-based OPC devices relying on four-wave mixing (FWM), a widely used approach to overcome the limitation on the launched pump power imposed by stimulated Brillouin scattering consists in imparting a phase modulation to the pump source so as to broaden the laser line-width, hence minimise the power spectral density integrated over the Brillouin bandwidth [4]. However, the pump phase modulation introduces phase distortions on the conjugated signal (idler) that can severely degrade the performance of phase-modulation signal formats [5]. In a dual-pump OPC system, the phase modulation transfer from the pump to the idler can in principle be fully suppressed by modulating the two pumps with the opposite phase modulation (push-pull) [6,7]. However, this approach involves adjustment of the delays and amplitudes of the electrical signals driving the phase modulators, which is difficult to perform exactly. Therefore, some residual dithering commonly exists in practice, even under carefully adjusted dithering settings [8], and appeals for the use of advanced digital signal processing (DSP) to counteract its side effects.

The majority of the existing DSP carrier phase recovery methods for high-order signal modulation formats have been developed to estimate and compensate the phase noise (PN) induced by laser nonzero spectral width in conventional coherent optical systems [9–11]. As a de facto standard in OPC-free systems, the feedforward blind phase search (BPS) (or minimum distance) carrier phase recovery method [9] can achieve a relatively good PN compensation effect and a high laser line-width tolerance. Furthermore, compared with pilot-aided (PA) PN compensation methods, blind methods can achieve higher spectral efficiency. Two-stage feedforward carrier recovery algorithms have also been introduced as a way of reducing the

required hardware effort and/or improving the line-width tolerance [12,13]. However, these traditional methods cannot efficiently counteract the deterministic effects of imperfections in the dithering scheme of OPC systems, because of either their blindness to the relationship between the phase modulation and the data signal [9] or the requirement of a relatively constant PN evolution over a long time window [11]. The frequency-domain peak searching (*m*th-power based) algorithm demonstrated in [14] to estimate the parameters of the pump dithering from the phase of the idler symbols before carrier phase recovery, in its original data-free implementation, performs poorly with nonuniform phase-distribution signals, therefore it is not suitable to high-order modulation formats.

Recently, various machine learning methods, such as supervised artificial networks, support vector machines and various types of unsupervised machine-learning clustering have been introduced in coherent optical communications to mitigate nonlinear transmission impairments or transceiver imperfections (see, e.g., [15] and references therein). Kernel methods form a powerful, versatile unifying framework to solve nonlinear problems in signal processing and machine learning [16]. These techniques are based on the implicit nonlinear transformation of the data from the input space into a high-dimensional inner product space or reproducing kernel Hilbert space, where the mapped data points are linearly separable, allowing classical linear methods to be applied directly on the data. In particular, kernel-based adaptive filtering (KAF) techniques are online kernel methods that aim to recover a signal of interest by adapting their parameters as new data become available, typically by minimising a least-squares (LS) cost function [17]. The computational complexity of these methods strongly depends on the size of the dictionary used to approximate the desired output, which can be curtailed by applying different sparsification or fixed-budget approaches. The majority of KAF techniques can be categorised into either least-mean squares techniques, which have linear complexity in terms of the stored data, or recursive LS (RLS) based techniques with quadratic complexity. In this paper, we deploy the sliding-window kernel-based RLS (KRLS) algorithm proposed in [18] to correct the phase distortion caused by deviations from ideal pump counter-dithering in the OPC of quadrature-amplitude modulation (QAM) signals [19]. In this approach, the phase of the signal after conventional pilot-free PN compensation is regarded as the result of a time-varying process. The online algorithm then tracks these time variations by considering data in windows of fixed size and calculating the updated solution for each window. Contrary to recently demonstrated dithering compensation methods [20], the approach used here requires no prior knowledge of the dithering frequencies and features high sensitivity to the residual pump dithering. The latter characteristic makes it particularly suitable for offsetting small imperfections in the pump-phase modulation scheme of OPC-assisted coherent systems. The proposed KRLS-based technique is verified experimentally and numerically with a 28-Gbaud dual-polarisation 16-QAM signal within an optical back-to-back OPC configuration, and shown to achieve a signal-to-noise (SNR) improvement of 0.4 dB relative to the BPS approach under optimised pump dithering settings in the OPC, and to tolerate pump-phase mismatch levels in a small to moderate strength range with negligible penalty relative to the optimum case. We also evaluate the performance of the scheme in a transmission setup with mid-link OPC through numerical simulations, and illustrate its applicability to the 64-QAM modulation format.

## 2. System description and methods

### 2.1. Experimental setup

The experimental setup of the dual-polarisation 28-Gbaud *M*-QAM system is depicted in Fig. 1(a). At the transmitter, ~ 60000 QAM symbols were generated for each polarisation. The data was then up-sampled at 2 samples per symbol and pulse-shaped using a root-raised-cosine filter with a roll-off factor of 0.1, loaded into an arbitrary waveform generator (AWG; 4-channel, 8-bit digital-to-analogue converter with 56-GSa/s sample rate from Keysight) and subsequently

converted into the optical domain by a commercial multi-format optical transmitter ( $\sim 100$ -kHz laser line-width on 192.4 THz). An erbium-doped fibre amplifier (EDFA) was used to control the launch signal power.

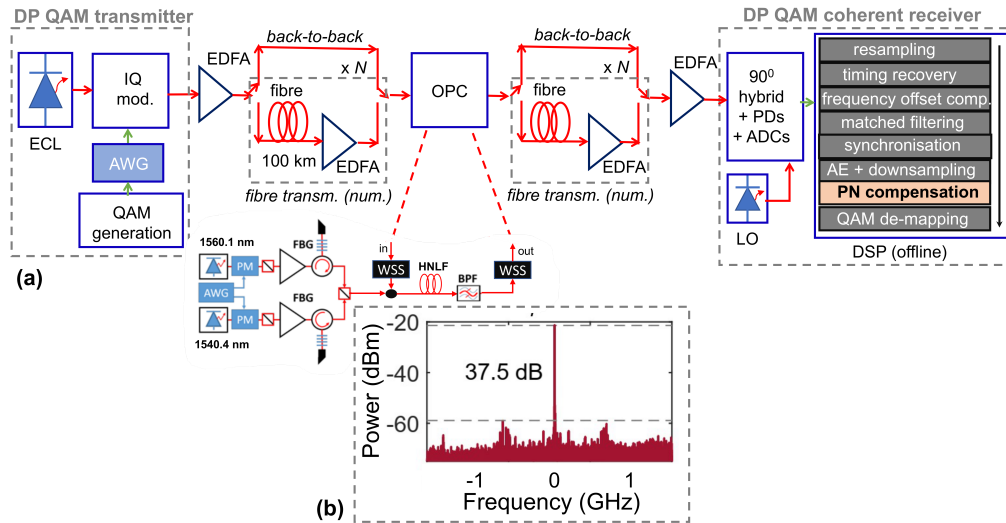


**Fig. 1.** (a) Experimental setup showing the dual-polarisation (DP) 28-Gbaud  $M$ -QAM transmitter, the dual-pump polarisation-independent OPC device, the coherent receiver, and the offline DSP equipped with the proposed kernel adaptive filtering PN compensation scheme. (b) RF spectrum of coherently received conjugated continuous-wave signal after the OPC with optimised pump dithering. ECL: external cavity laser, mod.: modulator, AWG: arbitrary waveform generator, EDFA: erbium-doped fibre amplifier, OPC: optical phase conjugation, PM: phase modulator, FBG: fibre Bragg grating, WSS: wave selective switch, BPF: optical bandpass filter, LO: local oscillator, PDs: photodetectors, ADCs: analogue-to-digital converters, AE: adaptive equaliser.

The signal was conjugated through a dual-pump polarisation-independent OPC [3,21] with orthogonally polarised pumps spectrally located at 1540.5 nm and 1560.1 nm, and with laser line-width  $\sim 30$  kHz. Two sets of two sinusoidal radio-frequency (RF) tones at frequencies  $f_1 = 60$  MHz and  $f_2 = 600$  MHz were generated by a two-channel AWG, amplified by RF amplifiers, and filtered by lowpass filters (LPFs) with a 3-dB bandwidth of 700 MHz to suppress the high-order intermodulation distortion resulting from the amplifiers' nonlinearity. The filtered RF tones were used to independently modulate the pumps via optical phase modulators driven in a counter-phasing fashion. The amplitude and phase parameters of the dithering tones were first adjusted in the AWG so as to minimise the phase modulation transfer to the idler, that is, to equalise the amplitudes of the pump phases and adjust the counter-dithering phase offset  $\delta\theta = \theta_2 - (\theta_1 + 180^\circ)$  to zero. Here,  $\theta_j$  denotes the phase of the tones driving each phase modulator  $j = 1, 2$ . Figure 1(b) shows the RF spectrum of the photo-detected conjugated copy of a continuous-wave laser after the OPC in these calibration settings. It features 37.5 dB suppression (relative to the carrier peak) of the phase-modulation sidebands transferred from the pumps. We refer to this operating condition as quasi-ideal pump counter-phasing. Then, we intentionally increased the phase mismatch  $\delta\theta$  by tuning the phase offset of the RF tones. The orthogonal pumps were amplified by two high-power EDFAs, filtered by fibre Bragg gratings with 1-nm 3-dB bandwidth to suppress the amplified spontaneous emission (ASE) noise around them, then combined with the signal and propagated in a highly nonlinear fibre (HNLF). The HNLF was 100-m long, and the values of the fibre nonlinear coefficient, zero-dispersion wavelength,

dispersion slope, and attenuation measured by the supplier were  $\gamma = 21.4 (\text{W} \cdot \text{km})^{-1}$ , 1550 nm, 0.041 ps/(nm<sup>2</sup> · km) and  $\alpha = 1.2$  dB/km, respectively.

Signal detection was performed using an intra-dyne coherent receiver, in which the conjugated copy of the signal was combined in a 90° optical hybrid with a local oscillator (~ 100-kHz line-width on 193.1 THz). Four balanced photodetectors were connected to the hybrid outputs, and real-time sampling scopes (100-GS/s sample rate, 33-GHz analogue bandwidth) were used as analogue-to-digital converters. A standard DSP procedure for data recovery [22] was implemented offline on a desktop computer. The DSP started with re-sampling the captured signal at 2 samples per symbol. Clock recovery and frequency-offset error correction were performed using a Gardner phase detector (window size of 1024) and a conventional Fourier transform-based method (window size of 4096), respectively. After matched filtering, frame synchronisation was achieved by use of the Schmidl-Cox algorithm [23]. An adaptive equaliser (21 filter-taps in the butterfly structure, with weights adapted every two samples through the constant-modulus algorithm) demultiplexed the dual-polarisation fields and compensated residual linear impairments. The signal was then down-sampled to 1 sample per symbol before being fed into the proposed PN compensation module described in Section 2.3. Two metrics were used to characterise the system's performance: the received SNR defined as  $\text{SNR} = \mathbb{E}_k[|x[k]|^2]/\mathbb{E}_k[|\hat{y}[k] - x[k]|^2]$ , where  $x[k]$  and  $\hat{y}[k]$  are the respective transmitted and received QAM symbols at the time instance  $k$  and  $\mathbb{E}$  is the expectation operator [24], and the bit-error rate (BER) obtained from direct error counting. We should note that the number of QAM symbols used in the experiment is insufficient to provide a statistically reliable BER estimation when the system's SNR is high, thus the number of errors is low. On the other hand, the use of the SNR metric is not applicable under strong dithering-induced PN due to its underlying Gaussian approximation.

## 2.2. Numerical model

The numerical model of the  $M$ -QAM system was implemented in Matlab. In the transmitter, a dual-polarisation 28-Gbaud QAM Nyquist shaped signal with a roll-off factor of 0.1 was simulated with 2<sup>20</sup> symbols per polarisation and 4 samples per symbol. The same number of samples were used in the transmission link, while the signal was up sampled at 224 samples per symbol at the entrance of the OPC module to have a sufficiently large simulation bandwidth to contain the two pumps. The transmitter and receiver lasers had a line-width of 100 kHz. The received signal was down sampled at 2 samples per symbol and filtered using a matched filter. The receiver DSP was the same as that implemented in the experimental setup. Five simulation runs per point were performed with different random number seeds for each numerical study presented in Section 3.

In our model of OPC, the complex field envelope of the pump waves, which is assumed free from amplitude fluctuations, was expressed as  $A_{pj}(t) = \sqrt{P_{0j}} \exp\{i[\delta\phi_j(t) + \phi_{mj}(t)]\}$ ,  $j = 1, 2$ , where  $j$  is the pump index,  $P_{0j}$  is the pump power,  $\phi_{mj}$  represents the modulated phase, and  $\delta\phi_j$  represents a phase fluctuation exhibiting a simple Brownian motion (Wiener process) in which the increments obey a Gaussian probability distribution [25]. Likewise with the OPC device used in the experiment, the pumps were independently phase modulated with two sinusoidal signals with frequencies  $f_1$  and  $f_2$ . We accounted for nonlinearities of the RF power amplifiers by using a memoryless polynomial model [26] for the amplifier response to the two-tone input signal. The output waveforms from the amplifiers were then filtered using LPFs as in the experiment. Therefore, the signals driving the phase modulators are given by [20]

$$\begin{aligned} \phi_{mj}(t) &= \int d\tau h(t - \tau) [\alpha_1 g_j(\tau) + \alpha_2 g_j(\tau)^2 + \alpha_3 g_j(\tau)^3], \quad j = 1, 2 \\ g_1(t) &= (m + \delta m) [\cos(2\pi f_1 t + \delta\theta) + \cos(2\pi f_2 t + \delta\theta)], \\ g_2(t) &= m [-\cos(2\pi f_1 t) - \cos(2\pi f_2 t)] \end{aligned} \quad (1)$$

where the  $\alpha$ 's are the coefficients of the polynomial response of the amplifiers, truncated to the third order and assumed identical for the two amplifiers,  $h(t)$  is the impulse response of the filters, assumed identical for the two filters,  $m$  is the modulation index, the modulation-index mismatch  $\delta m$  represents possibly different modulation indices, and the pump-phase mismatch  $\delta\theta$  accounts for a non-ideal phase shift. Since the envelope of the idler's field is proportional to the product  $A_{p1} \cdot A_{p2}$  [27], the general pump-phase contribution to the idler phase is given by  $\phi_{p \rightarrow i} = \phi_{p1} + \phi_{p2}$ , where  $\phi_{pj} = \delta\phi_j + \phi_{mj}$ . It is easy to see that the pump-phase modulation contribution only vanishes for ideal counter-phasing,  $\delta m = \delta\theta = 0$ , and further, under the assumption of linear amplifier response. This is difficult to achieve in practice. In our numerical simulations, we used  $m = 1.2$  rad,  $\delta m = 0.01$  rad,  $\alpha_1 = 1$ ,  $\alpha_2 = 0.007$ ,  $\alpha_3 = 0.005$ , where these values were chosen to match the measured continuous-wave idler's spectrum, and we varied the pump phase-mismatch parameter  $\delta\theta$  to control the deviation of the pump phases from optimum counter-phasing.

Each pump was combined with ASE noise from an amplifier and an optical bandpass filter was used to suppress the out-of-band noise around it. The pump waves, orthogonally polarised, were combined with the signal, polarised at a  $45^\circ$  angle with respect to either pump, and then sent to a HNLF. The numerical simulations of the field propagation in the fibre were based on two incoherently coupled nonlinear Schrödinger equations (Manakov system) [28] with the same parameters as those of the experimental setup. The nonlinear coefficient of the HNLF was adjusted slightly from the nominal value in order to match the experimentally observed conversion efficiency.

The fibre transmission link, depicted in Fig. 1, comprised  $N$  identical spans, each of 100-km standard single-mode fibre ( $\alpha = 0.2$  dB/km, dispersion coefficient =  $17$  ps/(nm · km),  $\gamma = 1.3$  (W · km) $^{-1}$ ) followed by an EDFA (6-dB noise figure) to compensate for the fibre loss. An OPC device was placed in the middle of the link.

### 2.3. Kernel adaptive filtering PN compensation method

Assuming perfect timing recovery, ideal synchronisation and zero frequency offset, the phase-distorted received signal at the input to the PN compensation unit can be written in the form

$$y[k] = x[k]e^{i(\delta\phi[k] + \phi_m[k])} + \varepsilon[k], \quad (2)$$

where  $\varepsilon[k]$  is the additive white Gaussian noise (e.g., ASE noise) present in the system. The first phase term represents the total Wiener random laser PN of the system:  $\delta\phi[k] = \delta\phi[k-1] + W[k]$ , where  $W[k] \sim \mathcal{N}(0, 2\pi\delta\nu T_s)$ ,  $\mathcal{N}(0, 2\pi\delta\nu T_s)$  denotes a normal distribution of mean 0 and standard deviation  $\sqrt{2\pi\delta\nu T_s}$ ,  $\delta\nu$  is a combined spectral line-width (total line-width of transmit, receive and pump lasers), and  $T_s$  is the symbol period [29]. The second phase term  $\phi_m[k] = \phi_{m1}[k] + \phi_{m2}[k]$  represents the deterministic phase distortion generated by imperfect pump counter-phasing (Eq. (1)). This is the phase component that we aim to track and compensate. As mentioned in the introduction, the effectiveness of the BPS-based carrier phase recovery method may degrade significantly under the impact of the dithering-induced PN term because of its direct decision operation. To circumvent this issue, we deployed an additional KAF compensation stage to aid the BPS algorithm, as depicted in Fig. 2(a). It is worth to note that to estimate the dithering-induced PN term we could perform linear regression using a Fourier basis. However, this approach would require knowledge of the exact frequencies. By contrast, the proposed kernel-based approach enables blind equalisation.

As mentioned in the introduction, kernel methods use positive definite kernel functions to operate in a high-dimensional, implicit feature space without computing the coordinates of the data in that space but rather by simply computing the inner products between the images of all pairs of data in the feature space [16,30]. A commonly used kernel function is the Gaussian kernel:  $k(\mathbf{x}, \mathbf{y}) = \exp[-\|\mathbf{x} - \mathbf{y}\|^2 / (2w^2)]$ , which implies an infinite-dimensional feature space. KRLS algorithms solve a LS problem in the feature space by inverting a kernel matrix  $\mathbf{K}$  whose

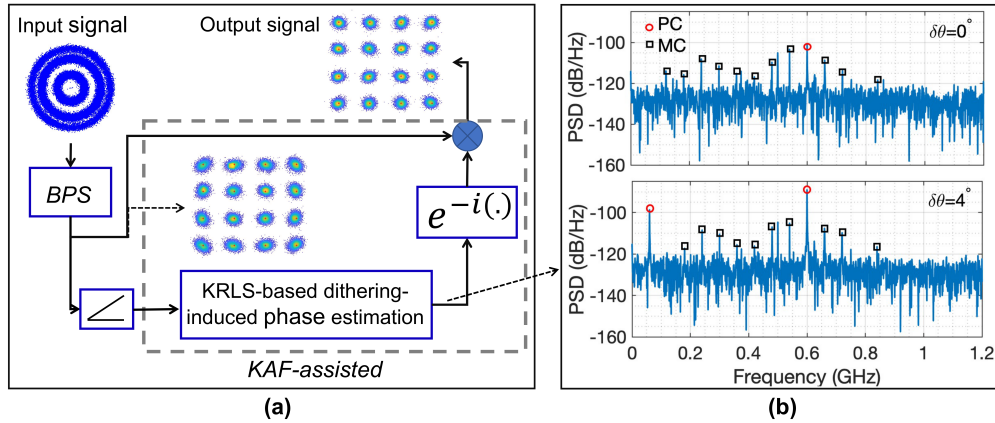


**Fig. 2.** (a) Block diagram of the proposed PN compensation scheme. (b) Spectral representation of the estimated PN after the KAF unit for 16-QAM. PC: Principal components (i.e., the RF frequencies), MC: mixing components.

elements are computed as  $\mathbf{K}(i, j) = k(\mathbf{X}_i, \mathbf{X}_j)$  where  $\mathbf{X}_i$  and  $\mathbf{X}_j$  are the  $i$ -th and  $j$ -th columns of the observation matrix, and whose dimensions therefore depend on the number of observations. The first KRLS-type algorithm proposed in the literature [31] limits the matrix dimensions by means of a sparsification procedure, which maps the samples to a limited dictionary. This permits both to reduce the order of the feature space which, in turn, prevents overfitting of the LS problem [32,33], and to keep the complexity of the algorithm bounded. Conversely, in the version of the KRLS algorithm proposed in [18], these two measures are obtained by two different mechanisms. On the one hand, overfitting is handled by regularising (penalising the norm of) the solution. On the other hand, the complexity of the problem is kept bounded by using a sliding-window approach in which only the observations in a window of fixed length,  $M$ , are considered, in combination with efficient matrix inversion formulae. The complexity of the problem is mainly determined by the calculation of the  $M \times M$  matrix  $\mathbf{K}_n^{-1}$  for each window of  $M$  data. In the update algorithm developed in [18], this is not done explicitly, but  $\mathbf{K}_n^{-1}$  is computed solely from knowledge of the data in the current window and the previous  $\mathbf{K}_{n-1}^{-1}$ , thereby maintaining an overall time and memory complexity of  $O(M^2)$  of the algorithm. The sliding-window KRLS algorithm is conceptually very simple and can obtain reasonable performance in a range of scenarios [34].

Within our proposed PN compensation scheme, the PN-distorted signal was first phase-compensated by the BPS algorithm, where we used a test-phase resolution of 32 and 64 phase angles for the 16-QAM and 64-QAM modulation formats, respectively [9]. We denote here the output signal from the BPS stage as  $\hat{\mathbf{Y}}_1$ . The signal phase was then stripped off and fed into the KAF unit whose operational principle relied upon the sliding-window KRLS algorithm presented in [18]. Slightly differently from [18], our implementation of the algorithm sought the optimal model vector  $\mathbf{h}$  that solved the LS problem

$$\min_{\mathbf{h}} \|\angle\{\lfloor \hat{\mathbf{Y}}_1 \mathbf{h} \rfloor_{\mathbb{D}}\} - \angle\{\hat{\mathbf{Y}}_1 \mathbf{h}\}\|^2, \quad (3)$$

where  $\angle\{\cdot\}$  and  $\lfloor \cdot \rfloor_{\mathbb{D}}$  are the angle and direct-decision operators, respectively. The remainder of the implementation followed Algorithm 1 in [18]. We used the common Gaussian kernel to calculate the elements of the kernel matrix, and we verified that the use of a different nonlinear kernel function, such as a periodic or polynomial kernel, did not affect the results. The choices of the length of the BPS block filter, sliding-window size  $M$ , regularisation constant  $c$  and width of the Gaussian kernel  $w$  are discussed in the following section. The so estimated evolution of

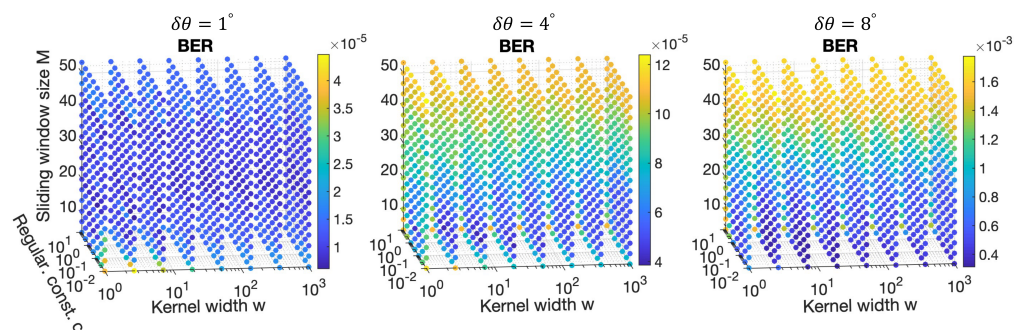
the phase was then used to compensate for the remaining phase distortion after the BPS block (Fig. 2(a)). Figure 2(b) shows examples of the estimated PN after the KAF unit in the frequency domain for 16-QAM at the pump-phase mismatches  $\delta\theta = 0^\circ$  and  $4^\circ$ , and  $\sim 36$ -dB optical SNR (OSNR). It is noteworthy that even in the optimum pump counter-phasing configuration, there are still several frequency components transferred from the RF tones and their linear and nonlinear mixing to the idler, indicating the persistence of some residual dithering. These components can be detected by the proposed KAF-assisted scheme. We also observe that the larger  $\delta\theta$  the higher the amplitude of these components.

Following the discussion above, execution of the KRLS algorithm in our PN compensation scheme brings about an  $O(M^2)$  computational complexity for each equalised QAM output symbol.

### 3. Results and discussion

The system for the back-to-back experiments was set to operate at an OSNR of  $\sim 36$  dB under optimum pump counter-phasing ( $\delta\theta \approx 0^\circ$ ) in the OPC device, which achieved an optimum effective SNR after DSP of  $\sim 21$  dB, indicating a transceiver noise-limited working regime [35]. Then we assessed the performance of PN compensation for varying pump-phase mismatch  $\delta\theta$ .

Following [9], the BPS filter length was set to 7 and 9 taps for the 16-QAM and 64-QAM systems, respectively. We chose a slightly smaller filter length for 16-QAM because at the high operational SNR of the system, the system's performance was dominated by PN and a smaller filter length yields higher PN estimation capability. The correct choice of the size  $M$  of the sliding window in the KRLS-based PN compensation scheme is very important for optimum performance of the method. Indeed, a too small  $M$  value may lead to overestimation of the PN in the solution updating process, whereas a too large  $M$  results in lessened PN compensation capability in like manner to the BPS method. To select the sliding window size, we used the direct-error count BER as the received SNR defined in Sec. 2.1 may be insensitive to phase overestimation. Figure 3 shows examples of scatter plots of the BER in the 3-dimensional space of kernel width  $w$ , regularisation constant  $c$  and sliding-window size  $M$  for the 16-QAM system in the presence of small, moderate and high residual pump dithering. We can see that a  $M$  between 7-8 and 14-15 works well for all dithering levels considered. Therefore, we can conveniently select the sliding window size to be equal to the BPS filter length, which simplifies the analysis by reducing the number of parameters to optimise in the implementation of the KRLS compensation scheme. We stuck to this choice in the remainder of the paper.



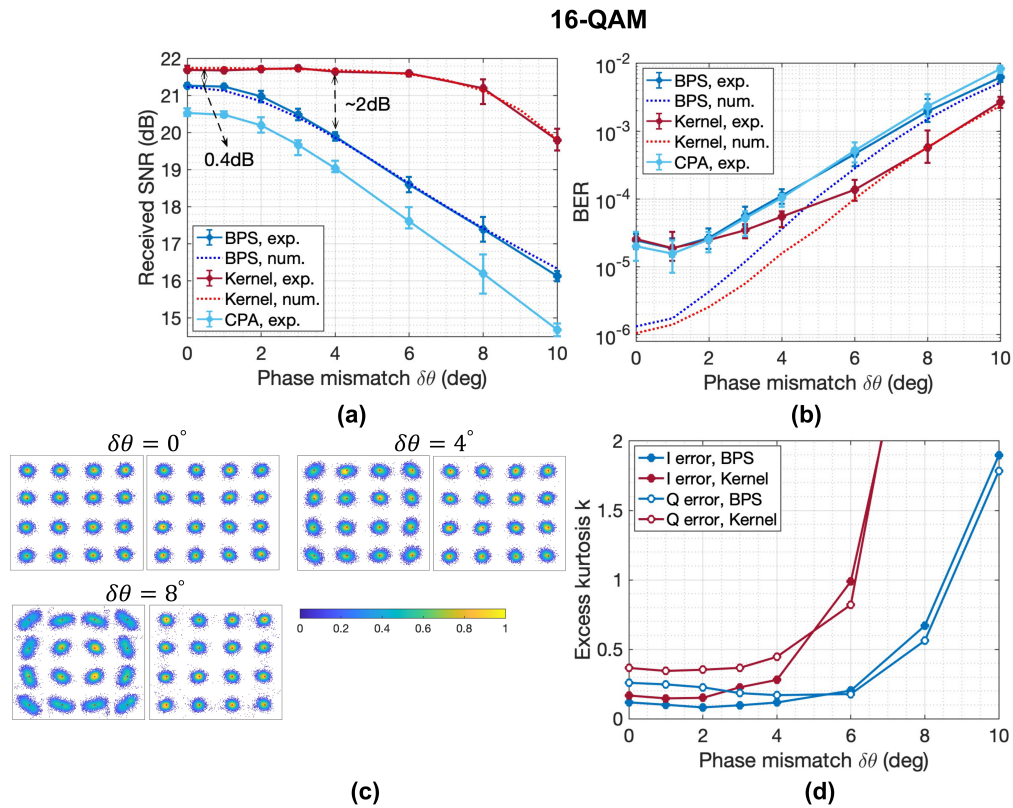
**Fig. 3.** Scatter plots of the direct-count BER in the 3-dimensional parameter space ( $w$ ,  $c$ ,  $M$ ) for the 16-QAM system at  $\delta\theta = 1^\circ$ ,  $4^\circ$  and  $8^\circ$  as obtained from experimental data.

Figure 4 summarises the PN compensation performance for the 16-QAM system. The kernel width and regularisation constant were set to  $w = 15$  and  $c = 0.5$  in the execution of the KRLS algorithm (see Fig. 7). We see in panel (a) that the performance of the conventional BPS

method degrades significantly under the impact of imperfect pump counter-phasing, where more than 1-dB SNR penalty is observed at a pump-phase mismatch of  $4^\circ$ . Conversely, the KRLS-based scheme gives 0.4 dB performance benefit over conventional BPS under the best pump dithering settings (i.e., at  $\delta\theta = 0^\circ$ ), and can tolerate pump-phase mismatches of up to  $6^\circ$  with negligible (less than 0.1-dB) penalty. Further, we observe that the SNR performance of the PN compensation schemes evaluated by numerical simulation of the model system matches very well the performance calculated from experimental data. The evolutions of the measured direct-count BER with the pump phase mismatch shown in Fig. 4(b) validate the SNR trends. However, we notice that the BER measured at  $\delta\theta = 0^\circ$  is worse than that recorded at  $\delta\theta = 1^\circ$  by use of either PN compensation method, while the corresponding error bars (which have lower and upper lengths equalling the minimum and maximum values, respectively, recorded over six independent data sets) still overlap. As mentioned in Section 2.1, the measured BER in the regime of small residual dithering where the system's SNR is high is not accurate due to the insufficient number of QAM symbols used. The numerical BER values match the experimental ones in the region of strong residual dithering, whilst they reach the range  $10^{-5} - 10^{-6}$  in the region of small to moderate dithering where the SNR is in the range 20 – 21.5 dB, which are close to the theoretically expected values. Importantly, the numerical simulations indicate that the KRLS method achieves a BER gain over the BPS method at all levels of residual dithering. The constellation diagrams recorded at  $\delta\theta = 0^\circ$ ,  $4^\circ$ , and  $8^\circ$  shown in Fig. 4(c) confirm that the phase errors are significantly reduced by application of kernel-based PN compensation as compared to the BPS scheme. Figure 4(d) describes the shape of the distribution of symbol positions on the received constellation diagrams after PN compensation as a function of the pump-phase mismatch by showing the evolutions of the excess kurtosis of the distributions of in-phase and quadrature errors, defined as the differences between received and transmitted symbols along the two quadrature dimensions. The excess kurtosis, defined as  $k = \mu^4/\sigma^4 - 3$ , where  $\mu$  and  $\sigma$  are the respective fourth central moment and standard deviation of the distribution, and 3 is the kurtosis of a normal distribution, measures the 'tailedness' of the distribution relative to a normal one [36]. We can see that the error distributions have positive excess kurtosis indicating heavier tails, hence the presence of more outliers, relative to a normal distribution of equal standard deviation. As one may infer from the constellation diagrams in Fig. 4(c), the distributions after KRLS compensation have smaller standard deviation than those after BPS, but their higher tails make them deviate from a Gaussian shape more than those after BPS. Notwithstanding, the excess kurtosis remains rather low (below 0.5) in the region of small to moderate residual dithering ( $0^\circ$  to  $4^\circ$ ) for both compensation methods, thus indicating that in this region the error distributions can still be approximated by normal ones, whereas it increases significantly for  $\delta\theta > 4^\circ$ . Therefore, we may conclude that the received SNR can be used as a reliable measure of the system's performance under small or moderate PN where the BER measurements are mostly inaccurate.

In Figs. 4(a) and 4(b), we have also plotted the performance curves for the one-stage conventional PA (CPA) method [11] (with a number of pilots per QAM symbol block optimised to 4). We can see that in the region of small to moderate pump-phase mismatches the PA scheme features a SNR degradation of  $\sim 1$  dB relative to its blind counterpart due to the scaling of the achievable SNR as the inverse product of laser line-width and symbol duration, while in the region of large  $\delta\theta$  its BER performance is comparable to that of the blind approach. These results confirm the efficiency of pilot-free PN compensation methods for 16-QAM systems.

We have also studied experimentally the performance of the KRLS-based PN compensation method when the 16-QAM system is operated at different OSNR levels. The results reported in Fig. 5 for pump-phase mismatches in the range  $0^\circ - 4^\circ$  show that the SNR achieved by the BPS method increases at a slower rate with the OSNR and deviates from a linear increase at lower OSNR levels with increasingly stronger residual pump dithering. Conversely, the performance of



**Fig. 4.** (a) Received SNR and (b) direct-count BER versus pump-phase mismatch  $\delta\theta$  for the 16-QAM system after BPS and KRLS-based PN compensation (blue and red curves, respectively). The experimental and numerical results are represented by solid and dotted curves, respectively. Also shown are the experimental performance curves after CPA compensation (light blue). (c) Constellation diagrams at  $\delta\theta = 0^\circ$ ,  $4^\circ$  and  $8^\circ$  for the BPS and KRLS-based schemes. (d) Excess kurtosis of the in-phase and quadrature error distributions on the received constellations after BPS and KRLS-based compensation (blue and red curves, respectively).

the KRLS stage is relatively insensitive to the pump-phase mismatch level, thereby leading to a SNR gain over the BPS stage which increases with higher OSNR and stronger residual pump dithering. In particular, we notice that for a given pump-phase mismatch, at the OSNR level where the SNR after BPS compensation is  $\sim 16.5$  dB – where 16.5 dB is the expected SNR at the pre-forward error correction (FEC) BER threshold of  $10^{-3}$  commonly used in numerical simulations –, the SNR gain of the KRLS method relative to BPS compensation is approximately a quarter of the gain achieved at the maximum baseline OSNR of  $\sim 36$  dB. The BER curves validate the SNR trends within their limitation at high SNR.

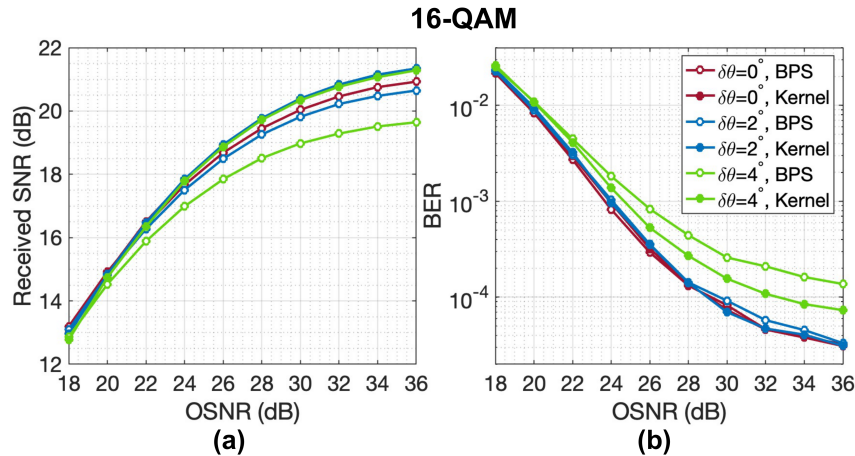


**Fig. 5.** (a) Received SNR and (b) direct-count BER versus OSNR for the 16-QAM system after BPS and KRLS-based PN compensation (open and closed circles, respectively) at  $\delta\theta = 0^\circ, 2^\circ$  and  $4^\circ$ , as obtained from experimental data.

As seen in panels (a) and (b) of Fig. 6, the situation changes notably for the 64-QAM system, which is operated close to its pre-FEC BER threshold under optimum dithering settings. The rate of decay of the SNR after BPS compensation with increasing pump-phase mismatch is higher than for 16-QAM, as expected considering the smaller PN tolerance of 64-QAM. The SNR and BER performances of the KRLS-based method (where we used  $w = 15$  and  $c = 5$ ) feature the same functional dependence on the pump-phase mismatch as the BPS performances, whilst retaining some advantage over their BPS counterparts across the whole range of  $\delta\theta$  values considered. The observed trends are reflected in the examples of constellation diagrams shown in Fig. 6(c), and explained by the high sensitivity of the solution update in the KRLS approach to wrong symbol decisions, which constrains the accuracy of PN estimation to the operating system's conditions of relatively high SNR and low impact of the dithering-induced PN. We can also see in Fig. 6 that the performance of the one-stage CPA method degrades with increasing pump-phase mismatch at a slower rate than that of the blind approach, either one-stage or two-stages (BPS + KRLS), yielding performance improvement over the blind approach in the region of moderate to high levels of residual pump dithering. These results indicate that an effective PN compensation in 64-QAM OPC-assisted systems requires the use of a two-stage PA scheme such as that proposed in [20].

Execution of KRLS algorithm requires knowledge of the parameters  $w$  and  $c$  which are not available analytically. In Fig. 7, we show the working ranges of parameter values within different SNR penalty constraints for the 16-QAM format and different pump-phase mismatch values. For each  $\delta\theta$  value we calculated the SNR penalty with respect to the maximum received SNR obtained at that phase mismatch as  $\max\{\forall \text{SNR}_{w,c}\} - \text{SNR}_{w,c}$ , where  $\text{SNR}_{w,c}$  is the SNR for a given parameter set ( $w, c$ ). The results in Fig. 7 highlight that there is considerable flexibility in

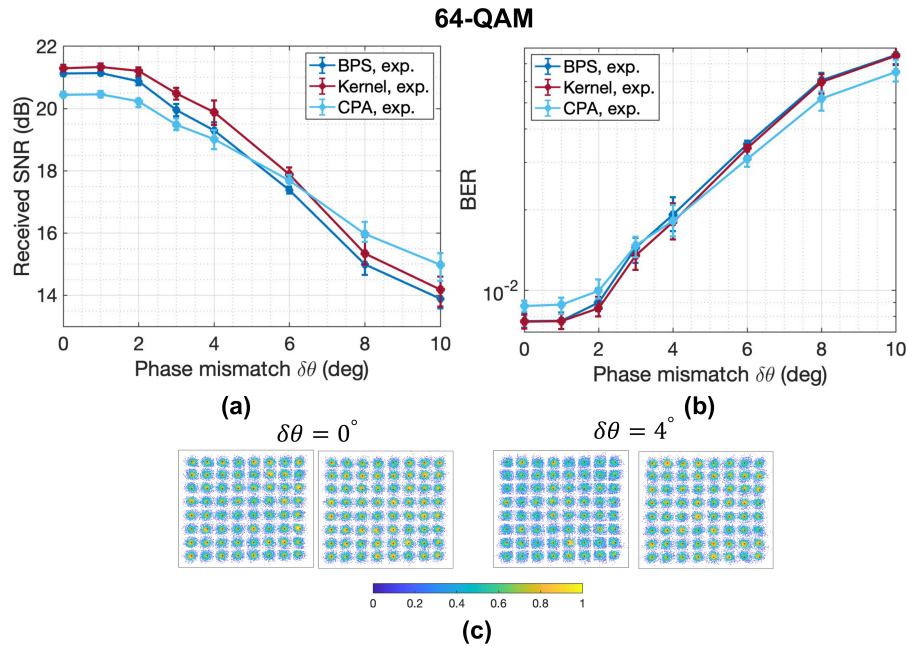


**Fig. 6.** (a) Received SNR and (b) direct-count BER versus pump-phase mismatch  $\delta\theta$  for the 64-QAM system after BPS and KRLS-based PN compensation (blue and red curves, respectively), as obtained from experimental data. Also shown are the experimental performance curves after CPA compensation (light blue). (c) Constellation diagrams at  $\delta\theta = 0^\circ$  and  $4^\circ$  for the BPS and KRLS-based schemes.

the choice of  $w$  and  $c$  subject to minor performance degradation. This stems from the adaptive operation of the kernel method. We can see in particular that there is a large overlap between the parameter regions bearing a SNR penalty of  $\leq 0.1$  dB (green areas) for every tested  $\delta\theta$  value but  $10^\circ$ . This means that the same set  $(w, c)$  can be chosen to feed the PN compensation scheme for different pump-phase mismatch levels.

We used numerical simulations to study the behaviour of our PN compensation scheme under a multi-span lumped amplification transmission configuration with mid-link OPC (Section 2.2). The length of the BPS block filter was set to 10 taps for 16-QAM and 11 taps for 64-QAM to accommodate the range of launched signal powers up to the maximum transmission length considered. The latter was chosen as the distance in the link at which the effective SNR after DSP was  $\sim 16.5$  dB for 16-QAM and  $\sim 19.5 - 20$  dB for 64-QAM at the optimum launched power (defined as the power yielding the highest SNR) and under the best dithering settings in the OPC ( $\delta\theta = 0^\circ$ ) – where 19.7 dB is the expected SNR value of 64-QAM at the pre-FEC BER threshold of  $10^{-2}$ . The parameters of the KRLS scheme were set to  $M = 10$ ,  $w = 50$  and  $c = 5$  for 16-QAM, and  $M = 11$ ,  $w = 50$  and  $c = 10$  for 64-QAM. Figure 8 shows the PN compensation performance in terms of received SNR and direct-count BER as a function of the transmission length, recorded at the optimum launched power for small to moderate residual dithering levels in the OPC. By comparing Figs. 8(a) and 8(b) for the 16-QAM system with the back-to-back results shown in Figs. 4 and 5, one may see that at those transmission distances in the link where the SNR values after BPS for a given  $\delta\theta$  are close to the values attained in the back-to-back setup, the KRLS compensation method brings about a commensurate performance advantage over BPS. The benefit of the method diminishes with longer transmission, due to both the increasing inaccuracy of the direct decision with the accumulation of ASE noise and the

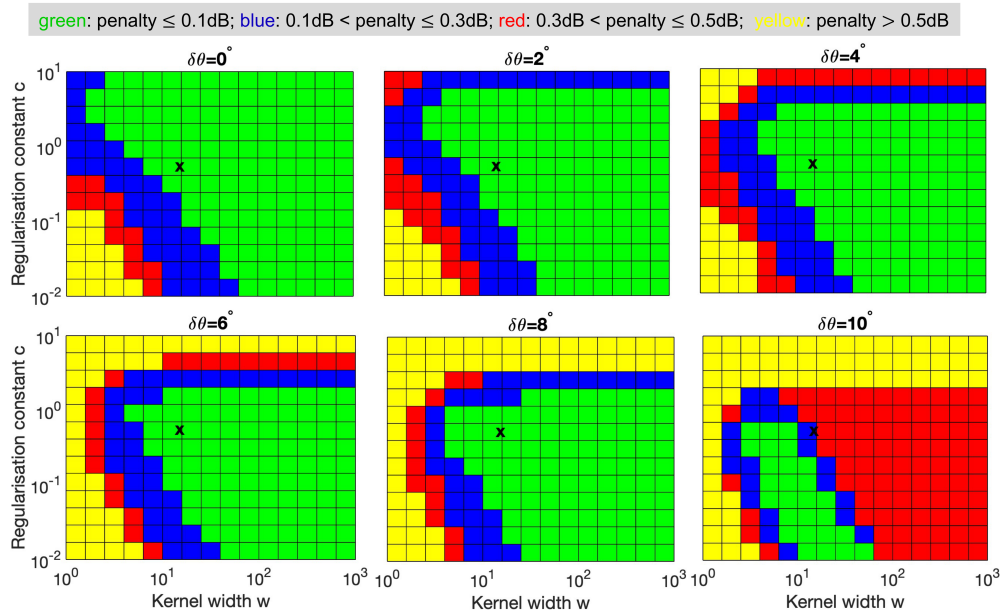


**Fig. 7.** Limits of operation of the KRLS-based PN compensation scheme under different SNR penalty constraints in the plane of kernel width  $w$  and regularisation constant  $c$  for 16-QAM and different values of the pump-phase mismatch  $\delta\theta$  as obtained from experimental data. The X marks indicate the parameter set  $(w, c)$  used in Figs. 4 and 5.

interaction of the chromatic dispersion of the second half of the link with the dithering PN, in an analogous way to equalisation-enhanced PN in conventional coherent systems [37]. Yet the SNR gain is at least 0.4 dB for all pump-phase mismatch values up to a transmission distance of 1600 km (where the system reaches its pre-FEC BER threshold for  $\delta\theta$  in the range  $2^\circ - 4^\circ$ ). Similar observations can be made about the 64-QAM system (Figs. 8(c) and 8(d)), while the working region of transmission lengths and residual dithering levels for which the KRLS method achieves appreciable SNR gain over BPS compensation is significantly reduced as compared to the 16-QAM system due to the faster growth of phase errors with increasing transmission distance and pump-phase mismatch. Figure 9 gives examples of the PN compensation performance in terms of BER as a function of the launched signal power. These examples were obtained after 16-QAM (64-QAM) transmission over 1200 km (600 km) of fibre link, respectively, where the system reached its pre-FEC BER threshold at  $\delta\theta$  in the range  $4^\circ - 6^\circ$  ( $2^\circ - 4^\circ$ ).

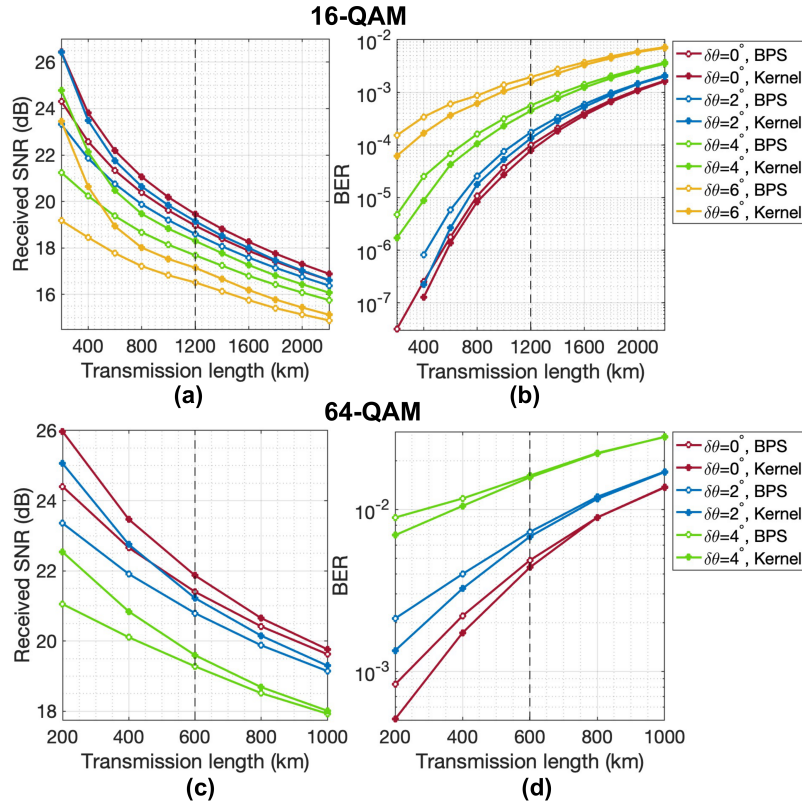


**Fig. 8.** Received SNR and direct-count BER after BPS and KRLS-based PN compensation versus length of the fibre link for (a, b) 16-QAM and (c, d) 64-QAM transmissions at the optimum launched power and different values of the pump-phase mismatch  $\delta\theta$ , as obtained from numerical simulations. The vertical dashed lines indicate the transmission distances at which the results in Fig. 9 were obtained.

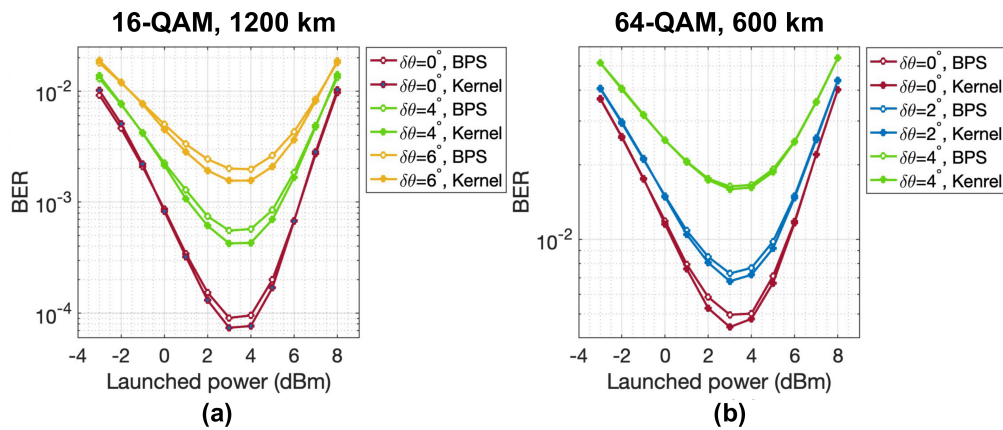


**Fig. 9.** Direct-count BER after BPS and KRLS-based PN compensation versus launched signal power for (a) 16-QAM transmission over 1200 km and (b) 64-QAM transmission over 600 km of fibre link at different values of the pump-phase mismatch  $\delta\theta$ , as obtained from numerical simulations.

#### 4. Conclusion

We have developed a PN compensation method enhanced by a KRLS algorithm that is able to estimate and correct the phase distortion arising from small imperfections in the pump-modulation scheme of OPC-assisted pilot-free coherent systems. Owing to the sensitivity of the solution update in the online algorithm to wrong symbol decisions, to obtain the full benefits of the method the system's SNR should be sufficiently high and the impact of the residual dithering PN should be relatively small. We have demonstrated that when used with 16-QAM signals, the proposed approach achieves SNR gain over conventional BPS-based PN compensation under fully optimised dithering settings and shows negligible performance penalty relative to the optimum case in the region of small to moderate residual dithering. Conversely, the application of the method to higher-order signal modulation formats such as 64-QAM is quite limited as a result of the decision-directed architecture of the BPS stage. Numerical simulations of a multi-span lumped amplification transmission setup with mid-link OPC have shown that the performance advantage over the BPS method under small or moderate dithering-induced PN is preserved in transmission, although the achievable performance gain diminishes with increasing transmission length.

In practical OPC devices it is impossible to completely eliminate the residual pump dithering. The ability to detect and correct the resulting phase distortion sets the technique presented in this paper apart from other residual dithering PN compensation methods [20]. Furthermore, owing to its non-parametric nature, the deployed KRLS algorithm is indifferent to the number of dithering frequencies used, which makes the present method potentially applicable to cascaded OPC systems.

**Funding.** UK Engineering and Physical Sciences Research Council ( EP/S003436/1 (PHOS), EP/S016171/1 (EEMC), EP/R035342/1 (TRANSNET)).

**Acknowledgments.** The authors would like to thank S. Takasaka and R. Sugizaki at Furukawa Electric Co. for supplying the HNLF used in the experiments.

**Disclosures.** The authors declare no conflicts of interest.

**Data availability.** Data underlying the results presented in this paper may be obtained from the authors upon reasonable request.

#### References

1. M. Morshed, L. B. Du, and A. J. Lowery, "Mid-span spectral inversion for coherent optical ofdm systems: Fundamental limits to performance," *J. Lightwave Technol.* **31**(1), 58–66 (2013).
2. A. D. Ellis, M. E. McCarthy, M. A. Z. Al-Khateeb, M. Sorokina, and N. J. Doran, "Performance limits in optical communications due to fiber nonlinearity," *Adv. Opt. Photonics* **9**(3), 429–503 (2017).
3. M. A. Z. Al-Khateeb, M. E. McCarthy, C. Sánchez, and A. D. Ellis, "Nonlinearity compensation using optical phase conjugation deployed in discretely amplified transmission systems," *Opt. Express* **26**(18), 23945–23959 (2018).
4. Y. Aoki, K. Tajima, and I. Mito, "Input power limits of single-mode optical fibers due to stimulated brillouin scattering in optical communication systems," *J. Lightwave Technol.* **6**(5), 710–719 (1988).
5. R. Elschner, C.-A. Bunge, B. Hüttl, A. G. i Coca, C. Schmidt-Langhorst, R. Ludwig, C. Schubert, and K. Petermann, "Impact of pump-phase modulation on fwm-based wavelength conversion of d(q)psk signals," *IEEE J. Select. Topics Quantum Electron.* **14**(3), 666–673 (2008).
6. M.-C. Ho, M. E. Marhic, K. Y. K. Wong, and L. G. Kazovsky, "Narrow-linewidth idler generation in fiber four-wave mixing and parametric amplification by dithering two pumps in opposition of phase," *J. Lightwave Technol.* **20**(3), 469–476 (2002).
7. R. Elschner, C.-A. Bunge, and K. Petermann, "Co- and counterphasing tolerances for dual-pump parametric  $\lambda$ -conversion of d(q)psk signals," *IEEE Photonics Technol. Lett.* **21**(11), 706–708 (2009).
8. M. A. Z. Al-Khateeb, M. Tan, M. A. Iqbal, A. Ali, M. E. McCarthy, P. Harper, and A. D. Ellis, "Experimental demonstration of 72% reach enhancement of 3.6 tbps optical transmission system using mid-link optical phase conjugation," *Opt. Express* **26**(18), 23960–23968 (2018).
9. T. Pfau, S. Hoffmann, and R. Noé, "Hardware-efficient coherent digital receiver concept with feedforward carrier recovery for m-qam constellations," *J. Lightwave Technol.* **27**(8), 989–999 (2009).
10. G. Colavolpe, T. Foggi, E. Forestieri, and M. Secondini, "Impact of phase noise and compensation techniques in coherent optical systems," *J. Lightwave Technol.* **29**(18), 2790–2800 (2011).

11. S. Randel, S. Adhikari, and S. L. Jansen, "Analysis of rf-pilot-based phase noise compensation for coherent optical ofdm systems," *IEEE Photonics Technol. Lett.* **22**(17), 1288–1290 (2010).
12. T. Pfau and R. Noé, "Phase-noise-tolerant two-stage carrier recovery concept for higher order qam formats," *IEEE J. Sel. Top. Quantum Electron.* **16**(5), 1210–1216 (2010).
13. J. H. Ke, K. P. Zhong, Y. Gao, J. C. Cartledge, A. S. Karar, and M. A. Rezaia, "Linewidth-tolerant and low-complexity two-stage carrier phase estimation for dual-polarization 16-qam coherent optical fiber communications," *J. Lightwave Technol.* **30**(24), 3987–3992 (2012).
14. R. Elschner, T. Richter, L. Molle, C. Schubert, and K. Petermann, "Single-pump fwm-wavelength conversion in hmlf using coherent receiver-based electronic compensation," in *36th European Conference and Exhibition on Optical Communication (ECOC)* (IEEE, 2010), pp. 1–3.
15. H. Mrabet, E. Giacumidis, and I. Dayoub, "A survey of applied machine learning techniques for optical ofdm based networks," *Trans. Emerging Tel. Tech.* **33**(4), e4400 (2022).
16. B. Scholkopf and A. J. Smola, *Learning with Kernels, Support Vector Machines, Regularization, Optimization and Beyond* (MIT Press, 2001).
17. W. Liu, J. C. Principe, and S. Haykin, *Kernel Adaptive Filtering: A Comprehensive Introduction* (Wiley, 2010).
18. S. V. Vaerenbergh, J. Vía, and I. Santamaría, "A sliding-window kernel rls algorithm and its application to nonlinear channel identification," in *International Conference on Acoustics, Speech and Signal Processing (ICASSP)*, (IEEE, 2006), pp. 789–792.
19. T. T. Nguyen, S. Boscolo, A. A. I. Ali, M. Tan, T. Zhang, S. Takasaka, R. Sugizaki, S. Sygletos, and A. D. Ellis, "Kernel-based learning-aided phase noise compensation in dual-pump optical phase conjugation coherent system," in *Optical Fiber Communication Conference and Exhibition (OFC)*, (OPTICA, 2021), p. M5F.6.
20. T. T. Nguyen, S. Boscolo, A. A. I. Ali, S. Sygletos, S. Takasaka, R. Sugizaki, and A. D. Ellis, "Digital compensation of imperfect pump counter-phasing induced phase distortion in optical phase conjugation of high-order qam," *Opt. Express* **29**(11), 17464–17475 (2021).
21. A. A. I. Ali, M. Al-Khateeb, T. Zhang, F. Ferreira, and A. D. Ellis, "Enhanced nonlinearity compensation efficiency of optical phase conjugation system," in *Optical Fiber Communication Conference and Exhibition (OFC)* (OPTICA, 2019), pp. 1–3.
22. S. J. Savory, "Digital filters for coherent optical receivers," *Opt. Express* **16**(2), 804–817 (2008).
23. T. M. Schmidl and D. C. Cox, "Robust frequency and timing synchronization for ofdm," *IEEE Trans. Commun.* **45**(12), 1613–1621 (1997).
24. R. Maher, A. Alvarado, D. Lavery, and P. Bayvel, "Increasing the information rates of optical communications via coded modulation: A study of transceiver performance," *Sci. Rep.* **6**(1), 21278 (2016).
25. M. Lax, "Classical noise. v. noise in self-sustained oscillators," *Phys. Rev.* **160**(2), 290–307 (1967).
26. J. C. Pedro and S. A. Maas, "A comparative overview of microwave and wireless power-amplifier behavioral modeling approaches," *IEEE Trans. Microwave Theory Tech.* **53**(4), 1150–1163 (2005).
27. C. J. McKinstrie, S. Radic, and A. R. Chraplyvy, "Parametric amplifiers driven by two pump waves," *IEEE J. Sel. Top. Quantum Electron.* **8**(3), 538–547 (2002).
28. G. P. Agrawal, *Nonlinear Fiber Optics* (Academic Press, 2001).
29. E. Ip and J. M. Kahn, "Feedforward carrier recovery for coherent optical communications," *J. Lightwave Technol.* **25**(9), 2675–2692 (2007).
30. V. N. Vapnik, *The Nature of Statistical Learning Theory* (Springer-Verlag New York, Inc., 1995).
31. Y. Engel, S. Mannor, and R. Meir, "The kernel recursive least squares-algorithm," *IEEE Trans. Signal Process.* **52**(8), 2275–2285 (2004).
32. F. R. Bach and M. I. Jordan, "Kernel independent component analysis," *Journal of Machine Learning Research* **3**, 1–48 (2002).
33. D. R. Hardoon, S. Szedmak, and J. Shawe-Taylor, "Canonical correlation analysis: An overview with application to learning methods," *Technical Report CSDTR-03-02* (2003).
34. S. V. Vaerenbergh and I. Santamaría, "A comparative study of kernel adaptive filtering algorithms," in *IEEE Digital Signal Processing and Signal Processing Education Meeting (DSP/SPE)*, (IEEE, 2013), pp. 181–186.
35. T. T. Nguyen, T. Zhang, E. Giacoumidis, A. A. I. Ali, M. Tan, P. Harper, L. P. Barry, and A. D. Ellis, "Coupled transceiver-fiber nonlinearity compensation based on machine learning for probabilistic shaping system," *J. Lightwave Technol.* **39**(2), 388–399 (2021).
36. L. T. DeCarlo, "On the meaning and use of kurtosis," *Psychol. Methods* **2**(3), 292–307 (1997).
37. W. Shieh and K. P. Ho, "Equalization-enhanced phase noise for coherent-detection systems using electronic digital signal processing," *Opt. Express* **16**(20), 15718–15727 (2008).